Progress In Electromagnetics Research, Vol. 149, 45–54, 2014

Full-Wave Semi-Analytical Modeling of Planar Spiral Inductors in Layered Media

Yan-Lin Li and Sheng Sun*

Abstract—In this paper, we present a full-wave semi-analytical solution to calculate the self and mutual impedances of two coupled spiral inductors with rectangular cross sections. In low-frequency electromagnetism, the self and mutual impedance of planar spiral inductors can be obtained based on the eddy current approximation, where the displacement current is disregarded. As the frequency increases, the size of the system can be designed to be smaller. However, the displacement current becomes more important in inductively-coupled systems. By directly deriving the Maxwell's equations without the eddy current assumption, the obtained full-wave model could be applied to both homogeneous and planarly layered media for wireless power transfer systems. Compared to the traditional methods, the newly derived impedances show a considerable discrepancy at GHz frequencies for millimeter-sized inductors, indicating the significance of the displacement current if the operating frequency of wireless power transmission reaches the GHz-range.

Nomenclature

$\mathbf{E}$, $\mathbf{H}$: Electric and magnetic fields
$\delta(x)$: Dirac Delta function
ρ, φ, z: Coordinates of the cylindrical coordinate system
ρ_n, z_n: Radius and position of loop/coil n
ρ_{ni}, ρ_{no}: Inner and outer radii of coil n, see Fig. 3
σ: Conductivity
ε_0, μ_0: Permittivity and permeability of free space
ε_r, μ_r: Relative permittivity and permeability
B_m, D_m: The amplitudes of upgoing and downgoing waves in layer m
d_m: Location of layer m, see Fig. 3
$F(z, z_1)$: Propagation function in layered media
f, ω: Operation frequency and angular frequency
$H_0^{(1)}(x)$, $H_0^{(2)}(x)$: Hankel functions
I, J: Electric current and electric current density in a loop/coil
k, k_ρ, k_z: Wave number and its ρ and z components
k_m, k_{mz}: Wave number and its z component in layer m
t_m: Thickness of layer m, see Fig. 3

Received 24 July 2014, Accepted 21 August 2014, Scheduled 26 August 2014
* Corresponding author: Sheng Sun (sunsheng@ieee.org).
The authors are with the Department of Electrical and Electronic Engineering, The University of Hong Kong, Pokfulam Road, Hong Kong SAR, China.

w_n, h_n, s_n: Width, thickness and spacing of coil n, see Fig. 3

$Z_{mn}^{ij}, M_{mn}^{ij}, R_{mn}^{ij}$: Self ($i = j$ and $m = n$) or mutual impedance, inductance and resistance between coil m of inductor i and coil n of inductor j

$J_0(x), J_1(x)$Bessel functions of the first kind

1. INTRODUCTION

Analytical and semi-analytical solutions are possible and always preferable in the modeling of inductors with regular configurations, among which planar inductors with cylindrical symmetry and rectangular cross section are the most common case. In the literature, the inductance formulae can be derived from the magnetic coupling between two coaxial circular current filaments [1–3], the Neumann's formula [4, 5], or the approximate expressions based on the data-fitting technique [6, 7]. Previous research mainly focused on inductors with different shapes, coaxial and non-coaxial configurations, and simple background was assumed. In addition, the eddy current approximation was used for low-frequency electromagnetism, which could be utilized for medical implant applications [8], for example.

Recently, high-frequency operations are of great interest as the density of electronic circuits grows and the exploitation of usable high frequencies, such as terahertz (THz), has advanced considerably. For inductor-based converter, a more accurate model is needed to predict the substrate leakage currents in a large frequency range, from a few megahertz up to 4–5 GHz [9, 10]. For wireless power transmission (WPT) into dispersive tissue, the optimal frequency was reported to be above 1 GHz when the size of the transmit coil became much smaller than the wavelength [11–13]. Since the tissue can be considered as a low-loss dielectric, the ratio between the displacement current and the conduction current is characterized by $\omega\varepsilon/\sigma$. In high-frequency regime, $\omega\varepsilon$ is comparable to or even larger than σ, which means the displacement current is not negligible any more. Hence, a full-wave or full-wave model for a coupled inductor system should be established to solve the self and mutual impedances more accurately.

In [11, 14], the vertical magnetic dipole (VMD) model [15] was applied to describe a WPT system with two concentric loops. The electromagnetic fields, due to a current loop over planarly layered media, can be obtained by computing a series of *Sommerfeld integrals* (SIs). Note that VMD model is only suitable for tiny current loops without considering the cross-section, where approximate magnetic dipole sources were assumed. It implies that it cannot be directly applied on a current loop with relatively large size, and a practical case with the cross-section. Hence, a general analytical or semi-analytical model is urgently appealing for more practical cases, which might also be considered as a more accurate 3D benchmark for the available computational electromagnetic solvers.

To address the aforementioned issues, we propose a full-wave model to describe a system with two coupled planar spiral inductors. The transmitting and receiving inductors have N_1 and N_2 turns of coaxial planar circular coils with rectangular cross-sections, respectively, which are located in planarly layered media. The wave propagation through inhomogeneous media can also be modeled by incorporating both the eddy current and the displacement current terms in Faraday's law. Furthermore, the self and mutual impedances can be obtained by the filament method and the equivalent circuit theory, where the cross section influence of coils is also taken into account. Based on this full-wave framework, the high-frequency responses of self and mutual impedances (Z_{mn}^{ij}) of the coupled spiral inductors can be captured and modeled semi-analytically. To the best of our knowledge, the idea in [16] was firstly proposed for geophysical probing. In this work, it is the first attempt to derive the solution to the field radiated by a planar spiral inductor by involving the conductivity (σ) and the permittivity (ϵ) in an explicit form, and then incorporate the filament method [3] to investigate the wave propagation into inhomogeneous media. Therefore, the eddy current effect and the displacement current effect on the impedances of a coupled spiral inductor system can be captured simultaneously.

The remainder of this paper is organized as follows: the coupled inductor system is described and semi-analytical solutions of Z_{mn}^{ij} are derived in Section 2. In Section 3, the proposed solution is verified numerically based on a finite-element method, and different examples are demonstrated for both homogeneous and inhomogeneous layered media. Finally, this paper will be concluded by an overview in Section 4.

2. FORMULATIONS AND EQUATIONS

As shown in Fig. 1, the two coaxial spiral inductors are embedded in a planarly layered media. The layered media are vertically inhomogeneous, with the topmost and the bottommost layers being half-spaces, and characterized by μ, ε and σ. This model can be considered as a simplified WPT system used in implantable biomedical devices.

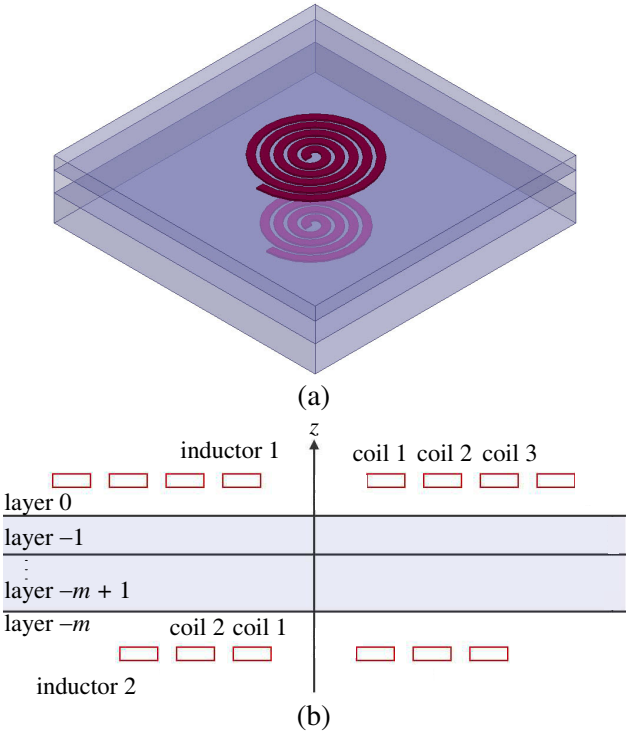

Figure 1. Spiral inductors with rectangular cross section in layered media: (a) 3-dimensional view, and (b) sectional view.

2.1. Formulation Using Filament Method

Assuming a time dependence $e^{-i\omega t}$ for all sources and fields, the electromagnetic fields due to an electric current source satisfy

$$\nabla \times \mathbf{H} + (i\omega\varepsilon - \sigma)\,\mathbf{E} = \mathbf{J_e}, \tag{1}$$

$$\nabla \times \mathbf{E} = i\omega\mu\mathbf{H}. \tag{2}$$

Considering $\mathbf{J_e}$ as a loop current source, only transverse electric (TE) modes can be excited because of the cylindrical symmetry. All the derivations below are assumed to be carried out in the cylindrical coordinate system. Following the procedure in [16, 17], (1) and (2) can be combined to be (3).

$$\left(\frac{\partial}{\partial\rho}\frac{1}{\rho}\frac{\partial}{\partial\rho}\rho + \frac{\partial^2}{\partial z^2} + \omega^2\mu\varepsilon + i\omega\mu\sigma\right) E_\phi = -i\omega\mu I\delta\left(\rho - \rho_1\right)\delta\left(z - z_1\right) \tag{3}$$

Letting

$$E_\varphi = \int_0^\infty dk_\rho k_\rho \tilde{E}_\phi J_1\left(k_\rho\rho\right), \tag{4}$$

we have

$$\left(\frac{\partial^2}{\partial z^2} + k_z^2\right)\tilde{E}_\varphi = -i\omega\mu I\delta\left(z - z_1\right)\rho_1 J_1\left(k_\rho\rho_1\right), \tag{5}$$

where $k^2 = \omega^2\mu\varepsilon + i\omega\mu\sigma$ and $k_z^2 = k^2 - k_\rho^2$. The solution of (5) is given by

$$\tilde{E}_\varphi = -\frac{\omega\mu I\rho_1 J_1(k_\rho\rho_1)\, e^{ik_z|z-z_1|}}{2k_z}, \tag{6}$$

and hence from (4) we can obtain (7),

$$E_\varphi(\rho, z) = -\frac{I\omega\mu\rho_1}{2}\int_0^\infty dk_\rho \frac{k_\rho}{k_z} J_1(k_\rho\rho)\, J_1(k_\rho\rho_1)\, e^{ik_z|z-z_1|} \tag{7}$$

which is the electric field generated by a current loop in free space. If the background consists of layered media, the propagation function in the integrand of (7), $e^{ik_z|z-z_1|}$, needs to be augmented by an upgoing wave plus a downgoing wave [15, 16]. For example, suppose the transmitter and receiver are placed in layer n and layer m, respectively. We have (8),

$$E_\varphi(\rho, z) = -\frac{I\omega\mu\rho_1}{2}\int_0^\infty dk_\rho \frac{k_\rho}{k_{0z}} J_1(k_\rho\rho)\, J_1(k_\rho\rho_1)\, F(z, z_1) \tag{8}$$

where

$$F(z, z_1) = e^{ik_{mz}|z-z_1|} + B_m e^{-ik_{mz}z} + D_m e^{ik_{mz}z}. \tag{9}$$

B_m and D_m can be solved recursively by applying constraint conditions at the boundaries of different layers [15, 16].

After $\mathbf{E}$ radiated by the source loop is determined, we can obtain the electromotive force (emf) introduced at the receiver loop, i.e.,

$$\mathcal{E} = \oint \mathbf{E}\cdot d\mathbf{l} = \int_0^{2\pi} \rho E_\varphi d\varphi = 2\pi\rho E_\varphi \tag{10}$$

According to the circuit theory, the mutual impedance between two loops can be defined as

$$\mathcal{E} = ZI = (R + i\omega M)\, I. \tag{11}$$

Obviously, Z is frequency-dependent, due to the frequency dependence of k_{mz}. Moreover, since both the effects of the eddy current ($\sigma\mathbf{E}$) and displacement current ($i\omega\varepsilon\mathbf{E}$) are taken into account in (1), this full-wave solution is practical and accurate for the high-frequency modeling. In the air, note that if the displacement current term in (3) is omitted, we have $k_z = -ik_\rho$ and hence

$$M = \pi\mu_0\rho\rho' \int_0^\infty dk_\rho J_1(k_\rho\rho)\, J_1(k_\rho\rho_1)\, e^{k_\rho|z-z_1|}, \tag{12}$$

which becomes the traditional formula of the mutual inductance between two filaments [1] without considering the displacement current term.

2.2. Impedances of Two Coupled Spiral Inductors

Similar to the previous procedure [3], the self and mutual impedances can be obtained based on the filament formulation and superposition theorem. First, let us consider the impedances between receiving coil m and transmitting coil n. For typical printed circuits, the metal thickness is normally on μm scale, and thus the aspect width to height ratio could be much larger than 1. As the dimension of the coils is far less than the wavelength, it is reasonable to assume the current density (J_φ) is inversely proportional to the filament radius ρ [3], i.e.,

$$J_\varphi(\rho, t) = \frac{Ie^{-i\omega t}}{\rho h \ln(\rho_o/\rho_i)}. \tag{13}$$

Since $dI = J_\varphi(\rho)\, d\rho dh$, (14) can be obtained by integrating (7) over the cross section of coil n,

$$E_\varphi(\rho, z) = -\frac{I\omega\mu}{2h_n \ln(\rho_{no}/\rho_{ni})}\int_0^\infty dk_\rho \frac{k_\rho}{k_{0z}} J_1(k_\rho\rho)\int_{\rho_{ni}}^{\rho_{no}} d\rho_1 J_1(k_\rho\rho_1)\int_{-\frac{h_n}{2}}^{\frac{h_n}{2}} dh e^{-ik_z|z-(z_n+h)|} \tag{14}$$

and further simplified by

$$\int_{\rho_{ni}}^{\rho_{no}} d\rho_1 J_1(k_\rho \rho_1) = \frac{J_1(k_\rho \rho_{no}) - J_1(k_\rho \rho_{ni})}{k_\rho}. \tag{15}$$

Similarly, following the routine in [3], the mutual impedance between these two coils is given by (16),

$$Z_{mn} = Z_0 \int_0^\infty dk_\rho \frac{[J_1(k_\rho \rho_{mo}) - J_1(k_\rho \rho_{mi})]\,[J_1(k_\rho \rho_{no}) - J_1(k_\rho \rho_{ni})]}{k_\rho k_{0z}} \int_{-\frac{h_m}{2}}^{\frac{h_m}{2}} d\tau_1 \int_{-\frac{h_n}{2}}^{\frac{h_n}{2}} d\tau_2 e^{-ik_z|(z_m+\tau_1)-(z_n+\tau_2)|}, \tag{16}$$

where

$$Z_0 = \frac{\omega \pi \mu}{h_m h_n \ln(\rho_{mo}/\rho_{mi}) \ln(\rho_{no}/\rho_{ni})}. \tag{17}$$

When the background is free space, the inner double integral can be solved analytically. For the layered media, since the exponential term in (15) is substituted by $F(z, z_1)$, the inner double integral has to be evaluated numerically. Then, the impedances between the inductors can be obtained by summing up all the coil impedances, i.e.,

$$Z^{ij} = \sum_{m=1}^{N_i} \sum_{n=1}^{N_j} Z_{mn}^{ij} \tag{18}$$

2.3. Sommerfeld Integral (SIs) Evaluation

The only difficulty to obtain the impedances lies in the slow convergence of Sommerfeld-type integrals involved in (7), (8), (14), (16). It is because the integrand includes highly oscillatory Bessel functions, slowly decaying exponential terms, as well as singularities introduced by k_{mz}. More specifically, the singularities are related to the $k_z^2 = k^2 - k_\rho^2$ dependence and vanishing denominator of the integrands [15, 18]. SIs have no closed-form solution and thus must be calculated numerically. The simplest way to evaluate SIs is deforming the Sommerfeld integration path (SIP) from the real axis into the complex k_ρ plane, by virtue of the Cauchy's theorem. On the other hand, the tabulation and interpolation method [19], discrete complex image method (DCIM) [20], and the steepest descent path (SDP) [15, 21] can also be applied to accelerate the convergence.

Here, the original SIP is deformed into the forth quadrant and divided into sub-paths with exponentially increasing length. Furthermore, Bessel functions are transformed using Hankel functions and the reflection formula:

$$\begin{cases} J_0(k_\rho \rho) = \dfrac{H_0^{(1)}(k_\rho \rho) + H_0^{(2)}(k_\rho \rho)}{2} \\ H_0^{(1)}(-x) = -H_0^{(2)}(x) \end{cases}. \tag{19}$$

In this way, the singularities are avoided and the asymptotic behavior of Hankel functions contributes to a fast convergence when the exponential damping in SIs is small.

3. NUMERICAL DEMONSTRATION

Since ε, σ and ω are all incorporated in the above formulation, both the dielectric loss and the displacement current effect at high frequencies can be captured. Here, the interested frequency range is in GHz for the *mm*-sized inductors, where the wavelength is much larger than the coil dimensions and thus (13) is guaranteed.

3.1. Field Distribution in Inhomogeneous Media

To verify our proposed solution, a two-half-space-layer problem is considered, where an electric current loop ($\rho_1 = 2\,\text{cm}$, $z_1 = 0$, $f = 1\,\text{GHz}$) lies $d = 1\,\text{cm}$ above a layer filled with lossy medium ($\varepsilon_r = 100$, $\sigma = 10$), as shown in Fig. 2(a). Fig. 2(b) and Fig. 2(c) show the semi-analytical and simulated $E_\varphi(\rho, z)$ line distributions along the vertical z- and horizontal ρ-directions, respectively. It

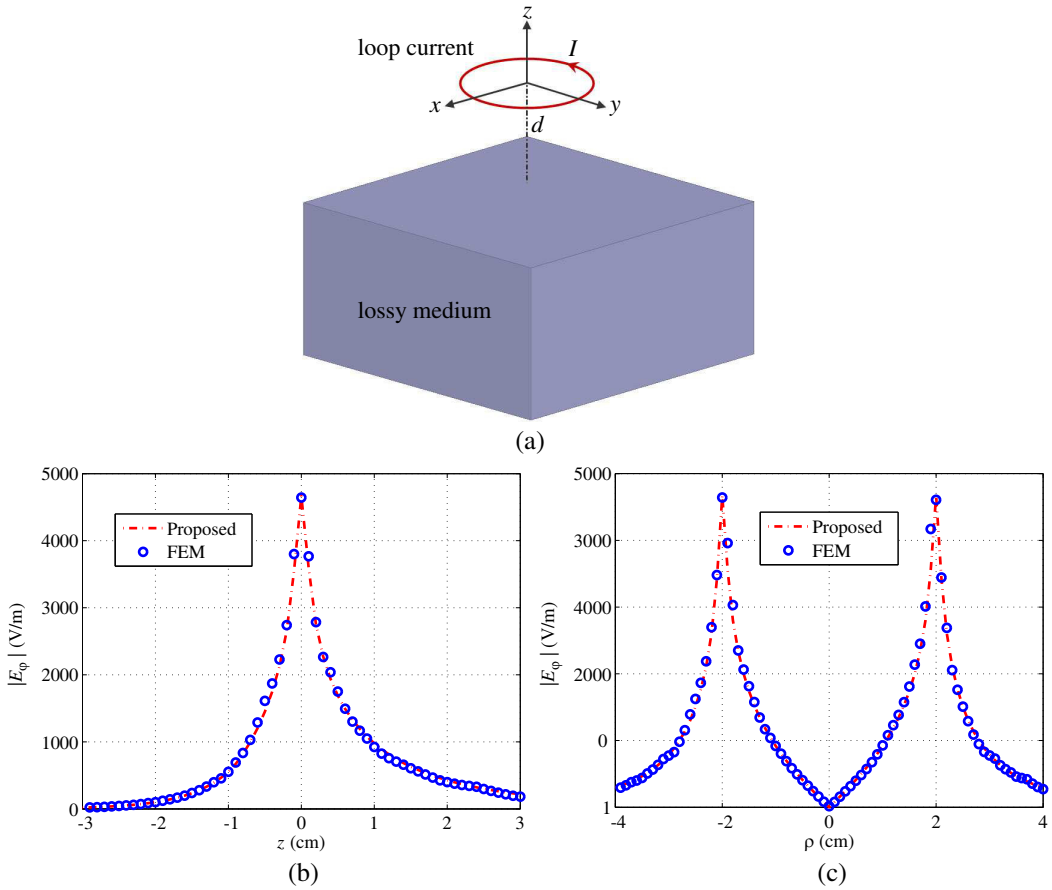

Figure 2. $E_\varphi(\rho, z)$ distribution of (a) a current loop along (b) line $\rho = 2\,\text{cm}$, $\varphi = 0$, and (c) $z = 0$, $\varphi = 0$.

can be noticed that the semi-analytical solutions obtained by (8) have good agreements with those obtained by the numerical method based on finite element method (FEM). It is interesting to observe that E_φ decays faster in the lower layer than that in the upper layer, due to the dielectric loss.

3.2. Impedances of Coupled Spiral Inductor Systems

Let us consider a more general inductively coupled system with two spiral inductors, as shown in Fig. 3. The dimensions are tabulated in Table 1. Here we only evaluate the mutual impedances between the two inductors, while the self-impedances can be obtained in the similar way. First, the air background is considered, as shown in Fig. 3(a). The calculated inductances and resistances in frequency range from 0.1 to 10 GHz are shown in Fig. 4. Also, Table 2 gives a quantitative comparison of the proposed and referred M^{21}. Note that the results obtained by the proposed method have a good agreement with those obtained by the eddy current assumption below 1 GHz. However, considerable discrepancy occurs at GHz frequency regime for both inductance and resistance. This is consistent with the physics that the M^{21} and R^{21} are frequency-dependent, and the displacement current becomes significant when the frequency becomes higher and the wave effect appears. Moreover, M^{21} reaches the maximum at $f = 6.31\,\text{GHz}$, which has a 56.0% discrepancy from the traditional calculation.

It should be pointed out that R^{ij}_{mn} is 0 because the expression of Z^{ij}_{mn} is previously purely imaginary [1] for an air background case. However, R^{ij}_{mn} is a nonzero value as Z^{ij}_{mn} is a complex number based on the proposed full-wave formulation. Note that at frequencies above 10 GHz, the wavelength becomes comparable to the inductor dimension, and thus (13) fails to approximate the real current distribution along the inductors. Fig. 4(b) shows a general sketch of the frequency-variant R^{21}.

Table 1. Dimensions for the spiral coils.

N_1	z_1	ρ_1	w_1	h_1	s_1
4	17.5 µm	0.5 mm	1 mm	35 µm	0.5 mm
N_2	z_2	ρ_2	w_2	h_2	s_2
3	−1.00175 cm	0.5 mm	1 mm	35 µm	0.5 mm

Table 2. Comparison between the proposed results and reference for M^{21} (nH).

	M_{11}^{21}	M_{12}^{21}	M^{21}
Reference	0.0016	0.0098	1.5712
Proposed ($f = 10^8$ Hz)	0.0016	0.0098	1.5717
Proposed ($f = 6.31 \times 10^9$ Hz)	0.0020	0.0119	2.4512

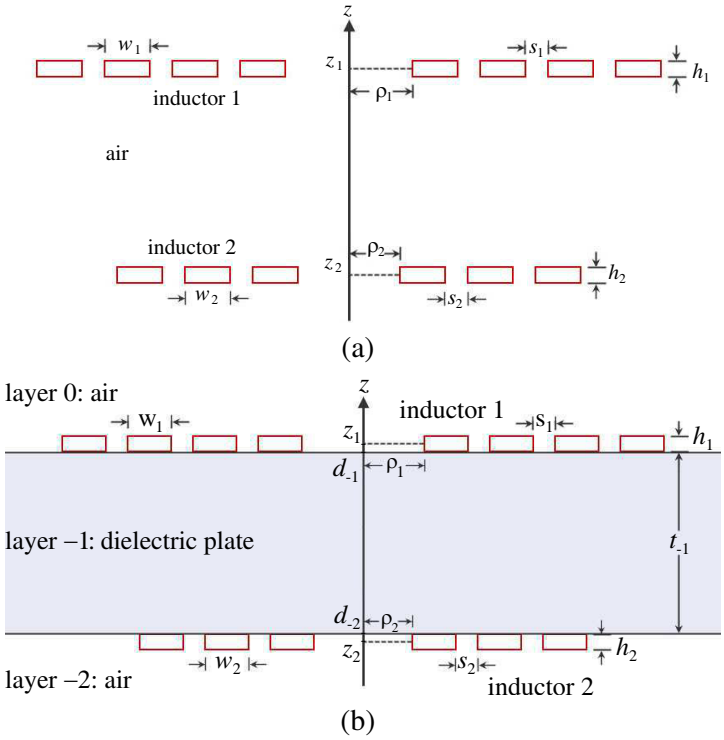

Figure 3. Spiral inductors embedded in (a) air and (b) layered media.

The proposed method can also be applied to the case with the presence of planarly layered media, based on the augmented propagation function. For simplicity but without loss of generality, 3-layer medium is considered. As shown in Fig. 3(b), the topmost layer (layer 0) and the bottommost layer (layer −2) are the air, while the middle layer (layer −1) is the dielectric.

To model the displacement current effect, $f = 1$ GHz, $\mu_r = 1.0$ and $\sigma = 0$ are assumed, while the other parameters maintain the same as shown in Table 1. Fig. 5 presents M^{21} and R^{21} as functions of ε_r for different values of thickness of layer −1. Results for air background case are also presented for reference. As ε_r increases, both M^{21} and R^{21} increase, then reach the maximum, and finally start to drop. Because $\sigma = 0$, it means there is no eddy current existing in the system. Thus, the oscillations are

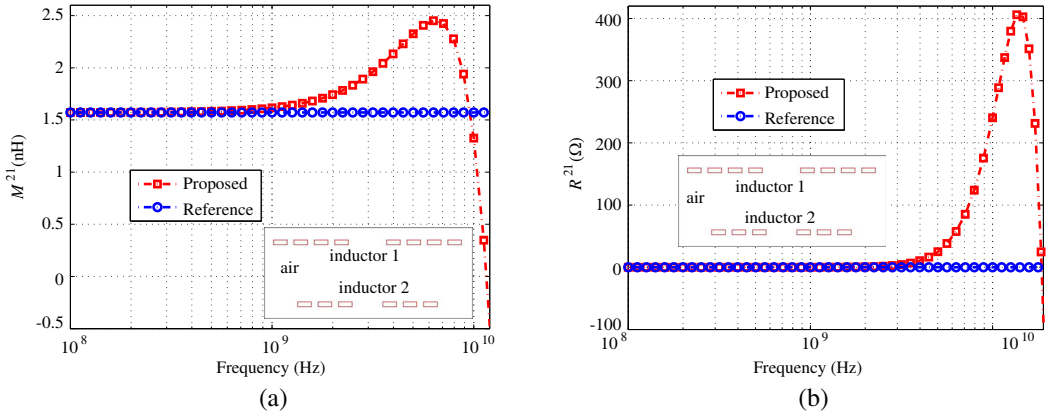

Figure 4. Mutual (a) inductances and (b) resistances of the system in air.

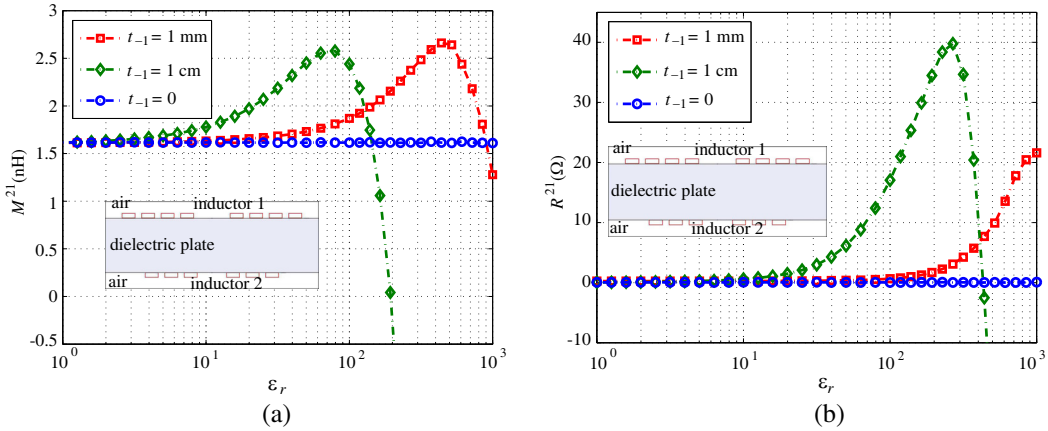

Figure 5. Mutual (a) inductances and (b) resistances of the system in inhomogeneous media.

Table 3. Comparison between the proposed result and reference for M^{21} (nH) and R^{21} (Ω).

	M^{21}		R^{21}	
	$f = 10^8$ Hz	Peak	$f = 10^8$ Hz	Peak
Reference	1.5708	-	0.0121	21.8706[a]
Proposed	1.5826	2.5347[b]	0.0124	70.8615[c]

[a] $f = 3.9811$ GHz; [b] $f = 1.0798$ GHz; [c] $f = 2.1544$ GHz.

mainly caused by the effect of the displacement current. In addition, the oscillations are advanced for the thicker dielectric layer, implying that the displacement current contribution is actually enhanced by high permittivity, which can be considered equivalently with a higher frequency, due to $k^2 = \varepsilon_r \mu_r \omega^2 / c^2$.

Finally, let us consider a muscle plate placed at layer -1, where the permittivity and conductivity vary with frequency and can be obtained by Debye relaxation model [11, 22]. The power transmission may bear radiation and dielectric loss at the same time. As shown in Fig. 6(a), the conductivity of muscle grows rapidly with frequency in the GHz range, while the permittivity begins to shrink. In Fig. 6(b) and Fig. 6(c), the frequency-variances of the mutual inductance and resistance for the system are illustrated, followed by a detailed comparison tabulated in Table 3. It is interesting to find that the results overlap at the beginning, and then diverge dramatically from each other as frequency increases. Since the displacement current contribution is discarded, the referred M^{21} drops monotonously. Note that the

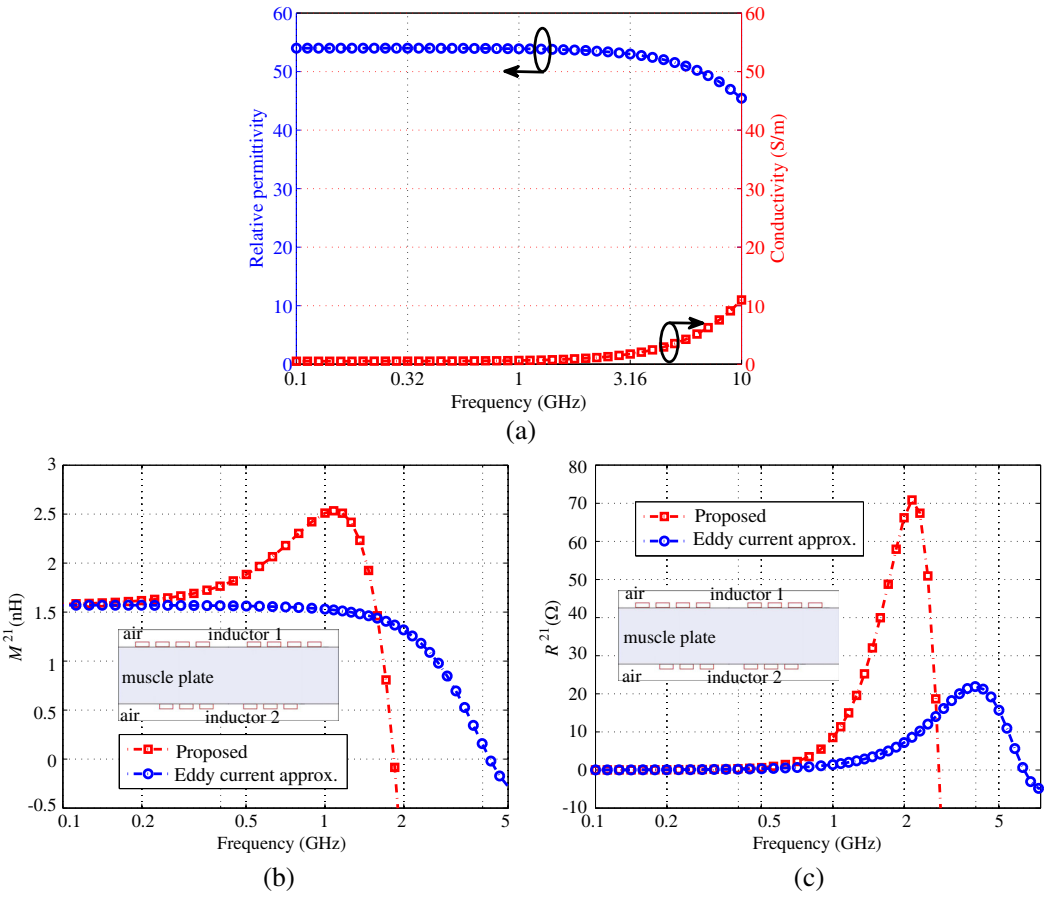

Figure 6. Mutual (b) inductances and (c) resistances of the system embedded by a muscle plate with frequency-varying (a) permittivity and conductivity.

maximum values of the proposed M^{21} and R^{21} can be found at $f = 1.0798\,\text{GHz}$ and $f = 2.1544\,\text{GHz}$, respectively. From the perspective of energy transmission efficiency, an optimal frequency can thus be deduced at GHz frequency range based on (11), which is consistent with the conclusion in [11].

ACKNOWLEDGMENT

This work was supported in part by the Research Grants Council of Hong Kong (GRF 716713, 716112), in part by the University Grants Council of Hong Kong (Contract No. AoE/P-04/08) and Seed Funding (201111159201 and 201211159076).

The authors would like to thank Prof. W. C. Chew of University of Illinois at Urbana-Champaign for the valuable discussions.

REFERENCES

1. Maxwell J. C., *A Trearise on Electricity and Magnetism*, Oxford Clarendon Press, 1873.
2. Grover, F. W., *Inductance Calculations*, Dover Publications, New York, 1946.
3. Hurley, W. G. and M. C. Duffy, "Calculation of self and mutual impedances in planar magnetic structures," *IEEE Trans. Magn.*, Vol. 31, No. 4, 2416–2422, 1995.
4. Zhong, G. and C. K. Koh, "Exact closed-form formula for partial mutual inductances of rectangular conductors," *IEEE Trans. Circ. Syst. Fund. Theor. Appl.*, Vol. 50, No. 10, 1349–1352, 2003.

5. Babic, S. I. and C. Akyel, "New analytic-numerical solutions for the mutual inductance of two coaxial circular coils with rectangular cross section in air," *IEEE Trans. Magn.*, Vol. 42, No. 6, 1661–1669, 2006.
6. Snow, C., *Formulas for Computing Capacitance and Inductance*, 544, National Bureau of Standards Circular, Washington, DC, 1954.
7. Mohan, S. S., M. Hershenson, S. P. Boyd, and T. H. Lee, "Simple accurate expressions for planar spiral inductances," *IEEE J. Solid-State Circuits*, Vol. 34, No. 10, 1419–1424, 1999.
8. Nguyen, M. Q., Z. Hughes, P. Woods, Y.-S. Seo, S. Rao, and J.-C. Chiao, "Field distribution models of spiral coil for misalignment analysis in wireless power transfer systems," *IEEE Trans. Microw. Theory Tech.*, Vol. 62, No. 4, 920–930, 2014.
9. Savio, A., M. Carmina, A. Richelli, L. Colalongo, and Z. M. Kovacs-Vajna, "A new lumped model for on-chip inductors including substrate currents," *Proceedings of the 15th International Conference on Microelectronics, 2003. ICM 2003*, 9–11, 2003.
10. Richelli, A., L. Colalongo, M. Quarantelli, M. Carmina, and Z. M. Kovács-Vajna, "A fully integrated inductor-based 1.8-6-V step-up converter," *IEEE Journal of Solid-State Circuits*, Vol. 39, No. 1, 242–245, 2004.
11. Poon, A. S. Y., S. O'Driscoll, T. H. Meng, "Optimal frequency for wireless power transmission into dispersive tissue," *IEEE Trans. Antennas Propag.*, Vol. 58, No. 5, 1739–1750, 2010.
12. Kim, S., J. S. Ho, and A. S. Y. Poon, "Wireless power transfer to miniature implants: Transmitter optimization," *IEEE Trans. Antennas Propag.*, Vol. 60, No. 10, 4838–4845, 2012.
13. Kim, S., J. S. Ho, and A. S. Y. Poon, "Midfield wireless powering of subwavelength autonomous devices," *Phys. Rev. Lett.*, Vol. 110, 203905, 2013.
14. Park, S. I., "Enhancement of wireless power transmission into biological tissues using a high surface impedance ground plane," *Progress In Electromagnetics Research*, Vol. 135, 123–136, 2013.
15. Chew, W. C., *Waves and Fields in Inhomogeneous Media*, IEEE Press, 1995.
16. Chew, W. C. and B. Anderson, "Propagation of electromagnetic waves through geological beds in a geophysical probing environment," *Radio Science*, Vol. 20, No. 3, 611–621, 1985.
17. Chew, W. C., S. Barone, B. Anderson, and C. Hennessy, "Diffraction of axisymmetric waves in a borehole by bed boundary discontinuities," *Geophysics*, Vol. 49, No. 10, 1586–1595, 1984.
18. Paulus, M., P. Gay-Balmaz, and O. J. F. Martin, "Accurate and efficient computation of the Green's tensor for stratified media," *Physical Review E*, Vol. 62, 5797–5807, 2000.
19. Tsang, L., C. Huang, and C. Chan, "Surface electric fields and impedance matrix elements of stratified media," *IEEE Trans. Antennas Propag.*, Vol. 48, No. 10, 1533–1543, 2000.
20. Dural, G. and M. I. Aksun, "Closed-form Green's functions for general sources and stratified media," *IEEE Trans. Microw. Theory Tech.*, Vol. 43, No. 7, 1545–1552, 1995.
21. Zhao, J. S., W. C. Chew, C. C. Lu, E. Michielssen, and J. M. Song, "Thin-stratified medium fast-multipole algorithm for solving microstrip structures," *IEEE Trans. Microw. Theory Tech.*, Vol. 46, No. 4, 395–403, 1998.
22. Gabriel, S., R. W. Lau, and C. Gabriel, "The dielectric properties of biological tissues: III. Parametric models for the dielectric spectrum of tissues," *Phys. Med. Biol.*, Vol. 41, No. 11, 2271–2293, 1996.